International Journal of Heat and Mass Transfer 118 (2018) 1243–1256

Contents lists available at ScienceDirect

International Journal of Heat and Mass Transfer

journal homepage: www.elsevier.com/locate/ijhmt

Boundary layer instabilities in mixed convection and diffusion flames with an unheated starting length

Colin H. Miller [a,*], Wei Tang [a], Evan Sluder [a], Mark A. Finney [b], Sara S. McAllister [b], Jason M. Forthofer [b], Michael J. Gollner [a,*]

[a] University of Maryland, Department of Fire Protection Engineering, 4356 Stadium Dr., College Park, MD 20742-3031, United States
[b] Missoula Fire Sciences Laboratory, US Forest Service, 5775 US Highway 10 W, Missoula, MT 59808-9361, United States

ARTICLE INFO

Article history:
Received 13 September 2017
Received in revised form 7 November 2017
Accepted 8 November 2017
Available online 22 November 2017

Keywords:
Boundary layer
Instability
Coherent structures
Laminar
Flame
Mixed convection
Streaks

ABSTRACT

The following study examines the role of streaklike coherent structures in mixed convection via a horizontal heated boundary layer possessing an unheated starting length. The three-dimensionality of flows in this configuration, which is regularly encountered in practical scenarios, has been experimentally probed using non-invasive detection methods. Experiments were conducted in a wind tunnel at the Missoula Fire Sciences Lab, and the wind speed was varied from 0.70 to 2.47 m/s. The buoyant source was varied significantly by either manipulating the surface temperature of a downstream hot plate or employing a diffusion flame. Streaks were visualized in the flow by means of infrared imaging or high speed video, and a novel detection algorithm was developed to quantify important properties and to spatially track these structures over time. Lognormal distributions of spacing were observed initially, and gradual deviations from this fit indicated a deviation from streaklike behavior. The onset of streaks was determined to be controlled by the pre-existing disturbances populating the incoming boundary layer. Further downstream, buoyant forces dominated the growth and deformation of these structures, whose length scale increased significantly. The width of structures was observed to asymptote to a stable value downstream, and this was determined to be a consequence of the finite distance over which heating was applied.

© 2017 Elsevier Ltd. All rights reserved.

1. Introduction

Forced and natural convection represent two distinct modes of heat transfer; however, many practical situations exist where both these mechanisms are influential. In these mixed convection scenarios, an understanding of both the buoyant force and the externally-induced flow field is essential to describing transport phenomena. One of the simplest examples of mixed convection is that of a boundary layer over a horizontal, heated plate. Here, the inertial force of the incoming wind is perpendicular to the upward force of buoyancy provided by the heat source. This scenario has been studied often since Pohlhausen's first solution for a laminar boundary layer over an isothermal plate [1], and many rich and complex features have been seen to complicate heat transfer predictions. In particular, streamwise streaklike structures have been observed in the near-wall region; after the onset of these vortices, the flow takes on a three-dimensional nature and heat transfer deviates from Pohlhausen's solution [2]. This behavior indicates that the applicability of a two-dimensional formulation may be limited; consequently, various researchers have examined streaks in heated boundary layers both experimentally and theoretically.

Gilpin et al. [2] conducted one of the first experimental studies on the onset of longitudinal structures over a horizontal flat plate, attempting to examine their effect on the validity of previous two-dimensional formulations [3–5]. They found that the location of the onset of vortices was correlated by the parameter $Gr_x/Re_x^{3/2}$. Other researchers have examined onset by means of a parameter of the form Gr_x/Re_x^n both experimentally [6–8] and analytically [9–13]. There is significant scatter in this data, owing at least in part to the inability of experiments to capture the earliest instances of small perturbations. Regardless, it has been shown that the presence of these streaks has a significant effect on modifying the heat transfer to the surface [14,6,7,15,16], indicating that the flow regime cannot be described by either forced or free convection. The presence of these structures are accompanied by a sudden increase in the boundary layer thickness [14], indicating a transition to a flow characterized by significant three-

* Corresponding author.
E-mail addresses: ubertus@umd.edu (C.H. Miller), mgollner@umd.edu (M.J. Gollner).

https://doi.org/10.1016/j.ijheatmasstransfer.2017.11.040
0017-9310/© 2017 Elsevier Ltd. All rights reserved.

dimensional effects [6]. Local velocity and temperature gradients exceed that predicted for a laminar boundary layer [6], and heat transfer rates can also be increased due to the secondary flow [16], which promotes the breakup of streaks and transition to turbulence. Streaks have been shown to have a large impact on local heat transfer rates during laminar-turbulent transition in inclined flow [17] as well as during breakup in natural horizontal convection [18].

The streaks observed in mixed convection over horizontal, inclined, or channel flows reportedly have some analogous behavior with Görtler vortices, which appear within a boundary layer forming over a concave wall. This is because both streaks in mixed convection over horizontal flows and Görtler vortices are affected by forces perpendicular to the flow direction [19]. Both instabilities are also manifestations of counter-rotating streamwise vortices in the near-wall region, which produce streaks by means of alternating upwash and downwash regions that significantly modify the spanwise velocity and temperature distributions [6,20,21].

Nevertheless, none of the previous studies on streaks in horizontal mixed convection have examined the effect of the leading edge. In inclined mixed convection, Zuercher et al. [22] have clearly demonstrated that the flow is incredibly sensitive to leading edge conditions. Configurations without an unheated starting length produced "unacceptable" effects, so a certain length of inert material was necessary to reproduce reliable flows. Unfortunately, nearly all of the previous experimental and theoretical studies on mixed convection in horizontal boundary layers appear to have neglected an unheated starting length. This not only raises questions about possible leading edge effects, but, in practical scenarios, mixed convection in boundary layers often exhibits an unheated starting length, such that the source of heat is located within a velocity boundary layer that has developed for some distance upstream. Examples can be found in a wide range of applications, including electronic cooling; chemical vapor deposition; process, geophysical, and atmospheric flows; and highly buoyant flows associated with boundary layer combustion, such as hybrid rocket engines, wildland fires, or pool fires. For this reason, it is highly desirable to obtain knowledge of streak behavior over flows with an unheated starting length, and this represents an important focus of the current study.

The original motivation for this problem comes from observations in wildland fires, which are fundamentally mixed convection problems possessing a strong source of local buoyancy. Although reacting flow adds another layer of complexity, it represents a realistic scenario where analogous behavior can be observed even at the extreme limits of local buoyancy. Coherent streamwise streaks have been observed in both flames and in smoke trailing the flame (see Fig. 1), a manifestation of counter-rotating vortices, which promote upwash and downwash regions [23]. Given recent findings that have supported convection as a dominant mechanism of preheating in wildland fire spread, there is reason to believe that the coherent structures observed in the flow field, including streaks, are important to heat transfer and thus the flame spread process [23]. Similar structures have also been observed in pool fires [24,25] and laboratory experiments [26,21]. Recently, Miller et al. [21] investigated the characteristics of flame streaks in a laminar boundary layer. Similar to previous findings in mixed convection, the streaklike structures significantly modified the spanwise distribution of gas temperatures and surface heat flux. Additionally, the streaks were seen to be preset by disturbances in the incoming boundary layer, and their growth was determined to be compatible with Rayleigh-Taylor Instabilities.

This study attempts to examine the analog between structures observed in strongly buoyant reacting flow and the more commonly-studied isothermal heated surface. The latter configuration, involving a heated surface, was chosen as a baseline experimental configuration because it is well-characterized and allows for the direct manipulation of the local source of buoyancy, which likely controls the growth of instabilities. Through adjustment of the wind speed and the surface temperature, the impact of inertia and buoyancy, which are the most common parameters of interest in a mixed convection experiment, can be assessed. The second experimental configuration, involving a boundary layer flame, does not enable direct manipulation of local buoyancy as a flame temperature is fixed. However, this experiment was chosen to probe the level of similarity in local instabilities at the extreme limits of buoyancy, which are commonly encountered in boundary layer combustion (including wildland fires). Finally, our experimental setup includes an unheated starting length so that further insights on the mechanisms of onset and growth of streaklike instabilities in mixed convection can be made.

2. Experimental setup and procedure

All experiments took place in the low speed wind tunnel facility at the Missoula Fire Sciences Laboratory. The wind tunnel is 3.0 × 3.0 m in cross-sectional area, 26.21 m in length, and is capable of reaching wind velocities of up to 3.12 m/s. The tunnel was operated under the recirculation operating mode, meaning that the air inlets and exhaust ports to the ambient were closed to avoid fluctuations from ambient winds and pressure changes. An environmental conditioning section was employed to maintain a desired temperature and humidity. Before each test, conditions were checked to ensure that air properties were not deviating significantly. Overall, conditions were held nearly constant at 19–22 °C and a relative humidity of 15–17%. Experimental wind speeds, as measured by a fixed centerline anemometer, were varied from 0.70–2.47 m/s.

A large horizontal platform, roughly resembling a table, was placed in the center of the wind tunnel, and its surface was 122 cm in width and 244 cm in streamwise length (see Fig. 2). A thin metal sheet (2-mm-thick) was fixed to the leading edge of this apparatus to minimize bluff body effects; this sheet's horizontal surface, which was 26 cm in streamwise length, remained flush with the downstream platform. An aerodynamic boundary layer would develop over the horizontal surface, beginning at the front edge of this metal plate. 188 cm downstream of this edge, a slot was made in which either a heated plate or a fuel wick could be placed. During hot plate experiments, a large copper plate (2.5-cm-thick, 20.5-cm-long, 91.5-cm-wide) was embedded flush with the horizontal surface along the centerline of the platform. The bottom of the copper surface made direct contact with three electric strip heaters (1500 W, 240 V), which provided uniform heating throughout the conductive plate. A K-type thermocouple was wedged securely between the copper plate and the surrounding insulation board to record the plate temperature via a temperature controller, which would regulate the plate temperature via on/off control. In experiments with flames, the copper hot plate was replaced by a porous ceramic fiber wick of identical dimensions (2.5-cm-thick, 20.5-cm-long, 91.5-cm-wide) placed 188 cm downstream of the leading edge of the apparatus. The wick was saturated with 400 mL of isopropyl alcohol and ignited using a torch.

The downstream edge of the plate (or fuel wick) was normalized as $x = 0$, the origin for streamwise coordinates, and this distinction will be maintained in all discussions of the hot plate. At this location, the Reynolds number (Re) varies from $8.7 * 10^4$ to $3.1 * 10^5$, depending on the ambient wind speed. This places the relevant portion of the experiment at the upper end of the laminar regime for flat plate flow, in which transition is typically observed at $Re \approx 5 * 10^5$.

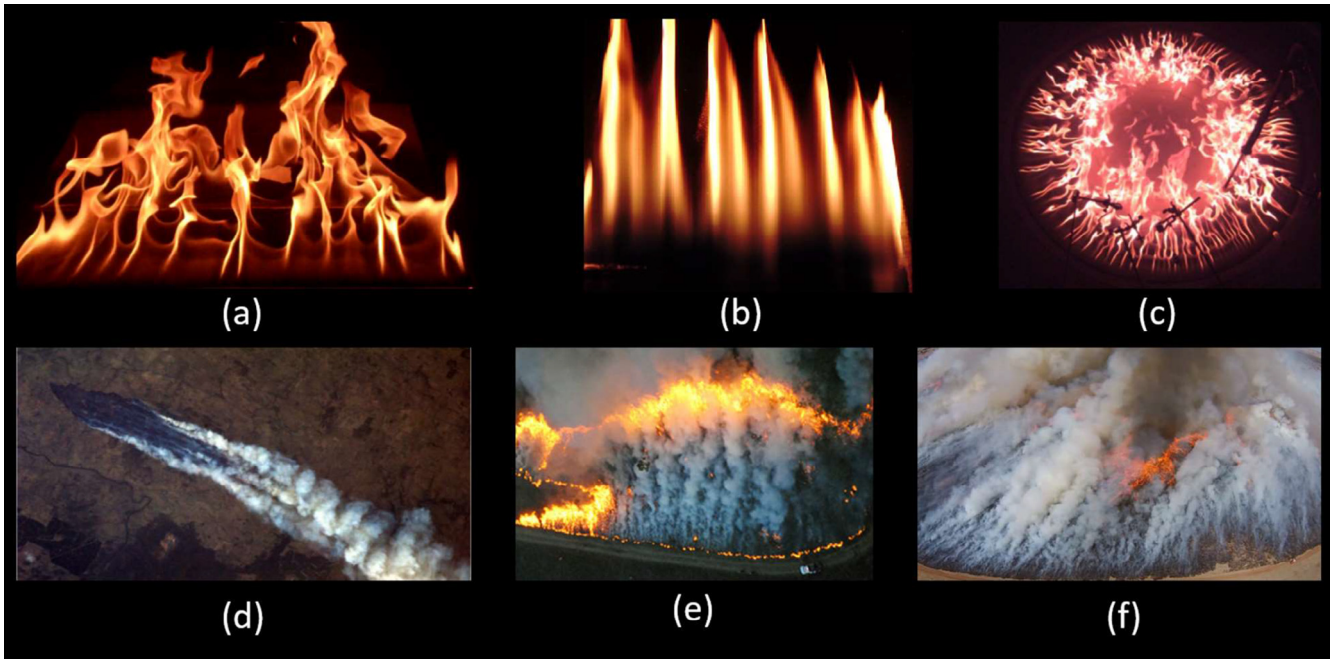

Fig. 1. Coherent structures in the form of streaks observed in wind-blown flames. Clearly visible streaky structures can be seen emanating from the leading edge of all these wind-blown flames. (a) Top view of flames from an inclined ethylene burner. (b) Top view of propane burner in crossflow reproduced from Miller et al. [21]. (c) Ring fire at Missoula Fire Sciences Laboratory. (d) View of Australian brush fire from International Space Station (Credit: NASA/Chris Hadfield). (e) Aerial view of flames and smoke from prescribed burn (NPS/John Nobles). (f) Closing the circle on a prescribed burn, Deerhead, KS (https://youtu.be/lcLnhs4FXvI).

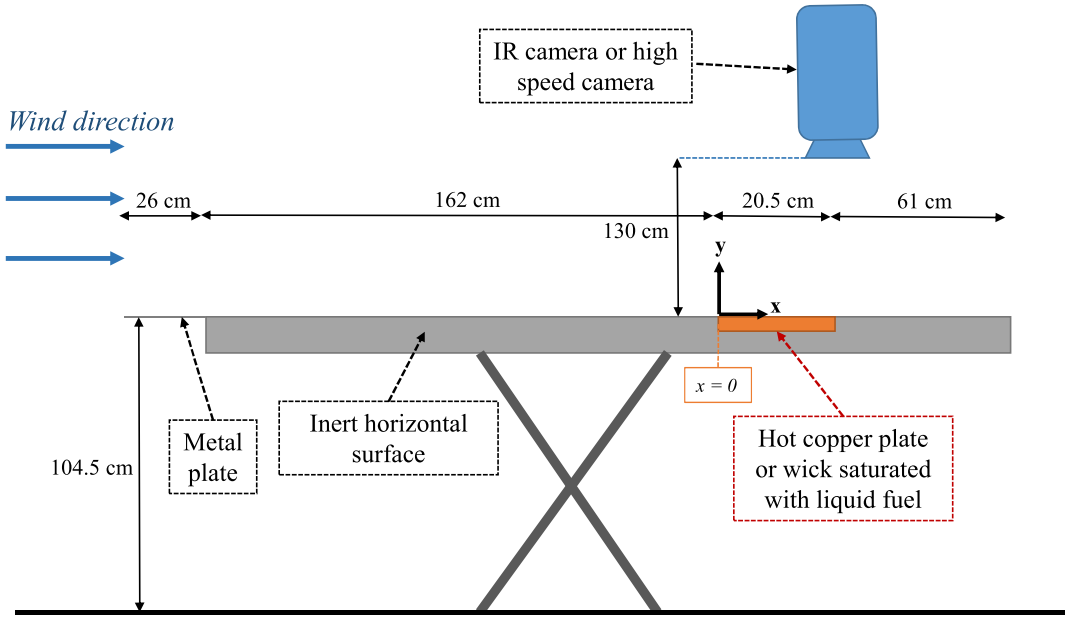

Fig. 2. Experimental schematic of hot plate apparatus at the Missoula Wind Tunnel Facility. This apparatus was located in the center of a wind tunnel with a 3.0 × 3.0 m in cross-sectional area.

The macroscopic properties of both non-reacting thermal plumes and boundary layer flames is generally understood to be governed by a competition between momentum and buoyancy. Consequently, the parameter space of this experiment consists in varying the strength of momentum through the ambient wind velocity or in controlling the power of buoyancy through the surface temperature of the hot plate. For the following experiments, the bulk wind speed was held at either 0.70, 1.27, 1.86, or 2.47 m/s (±0.04 m/s), while the buoyant force was provided either by a hot plate with a surface temperature of 150 or 300 °C or by an isopropyl diffusion flame.

In hot plate experiments, a FLIR SC6811 infrared camera was placed above the copper plate in order to measure surface temperatures. The wavelength range detected by the camera was 3–5 μm, and five separate filters were employed to span temperatures from 0 to 350 °C. An emissivity of 0.92 was assumed for both the copper plate and the surrounding insulation, which were painted black. The resolution of each image was 640 × 512 pixels covering a

region roughly 42 cm × 35 cm over the center of the plate and the region just downstream. Temperatures recorded by the IR camera likely deviate from actual values by a small margin; nevertheless, this was not a great concern since our goal was detection of transient changes in surface temperature as opposed to precise measurements of absolute value. Errors due to refraction from hot gases appeared to be minimal, as images of surface temperatures remained well-resolved over the duration of the experiment. For each temperature filter and parameter space, the surface temperatures were recorded at 280 Hz for a duration of approximately 15 s. In experiments with flames, 12 s of high speed (120 fps), high resolution (1080 × 1920 pixels) video footage were made from an overhead view.

Significant post-processing was necessary in order to detect streaks from infrared images or high speed video. Full details of this process are too lengthy to be enumerated within the body of this paper, but more detail on the detection algorithm can be found in the appendix (see Section A). Image processing was performed in MATLAB, and peak-detection methods were applied to spanwise profiles of either surface temperature fluctuations over the hot plate or luminosity profiles from the flame (see streak traces in Fig. 3). A variety of other methods have been employed by other researchers to look at streak properties, including visual inspection [27–32], spectral methods [33,34], and edge detection [35]. However, visual inspection is tedious and subject to human errors and biases. Spectral methods, which tend to employ Fourier transforms and autocorrelations, have been reported to be unreliable [35–37]. Edge detection methods appear to hold promise [35], but we selected peak-detection because it is intuitive and repeatable when applied to a single spanwise profile of temperature fluctuations. This algorithm enabled the tracking of streaks over time at various streamwise locations, and relevant data on properties such as streak spacing, width, meandering velocity, and amplitude could be extracted and tabulated at various streamwise locations. This enabled the repeatable and objective compilation of a significant dataset describing streak behavior.

3. Results

3.1. Velocity characterization

As a first step to characterizing the experiment, it is necessary to have some understanding of the incoming flow. For this reason, velocity measurements were taken in the region before the setup and just ahead of the hot plate. A TSI IFA 300 Constant Temperature Anemometer System was employed with a T-type thermocouple placed in the center of the wind tunnel to make sure temperature-based calibrations were accurate. All measurements were made at a frequency of 1000 Hz for a period of 65 s. All measurements were made in cold flow, meaning that neither the hot plate nor a burning fuel wick were active during velocity measurements. This was necessary because the hotwire would be unable to account for the high frequency temperature fluctuations associated with these heat sources.

The free stream velocity in the relevant portion of the wind tunnel was first characterized at the centerline of the wind tunnel 1.5 m upstream of the leading edge. The surface of the apparatus sits 104.5 cm above the wind tunnel floor, so measurements were made at heights of 95, 105, 115, and 125 cm in order to capture the portion of the flow relevant to the experimental area. Four wind speeds were tested and results are shown in Fig. 4. The average of all four measurements from one wind speed were used to determine the free stream velocity, U, which is indicated in the legend. The mean velocity varied minimally between heights, indicating a highly uniform flow across the height of the wind tunnel. Additionally, the flow was seen to be quite smooth, with turbulence intensity measurements on the order of 0.01%. These results indicate that the wind tunnel is well-conditioned and capable of providing repeatable incoming flow conditions for all experiments.

In addition to characterizing the bulk flow of the wind tunnel, the boundary layer forming over the experimental apparatus was also measured. Velocity profiles were assessed 1.5 cm upstream of the hot plate location, and measurement heights ranged from 3 to 200 mm. More spatial resolution was applied to the near-wall measurements in order to more properly characterize the shape of the boundary layer. Velocity measurements for all four wind speeds are displayed in Fig. 5. These results indicate that a boundary layer has clearly formed in the region upstream of the hot plate. Turbulence intensity profiles collapse when plotted against height, indicating that relative levels of velocity fluctuations are maintained throughout all tested boundary layers. Reported values for turbulence intensity do not exceed 1%, indicating minimal fluctuations.

In studies of boundary layers, scaling is often accomplished using a nondimensional wall unit [38]. This wall unit is a nondimensionalized quantity described by

$$y^+ = \frac{y u_\tau}{\nu}, \tag{1}$$

where y^+ is the distance in wall units, y is a relevant length, u_τ is the friction velocity and ν the kinematic viscosity. All properties were evaluated at a temperature of 20 °C. Here, the friction velocity is defined as

$$u_\tau = \sqrt{\frac{\tau_w}{\rho}}, \tag{2}$$

where τ_w is the wall shear stress and ρ is the density of air. Further, the wall shear stress is defined as

$$\tau_w = \mu \left.\frac{\partial u}{\partial y}\right|_{y=0}, \tag{3}$$

where μ is the dynamic viscosity, and $\left.\frac{\partial u}{\partial y}\right|_{y=0}$ the velocity gradient at the surface. From these equations, we can see that the wall unit is directly related to the velocity gradient near the wall. In such a way, this measurement becomes a useful way to quantify the boundary layer profile, particularly for the near-wall portion which is relevant to streak formation.

We applied this procedure to the velocity profile from Fig. 5 in order to determine the length of a nondimensional wall unit at the leading edge of the hot plate. For each wind speed, the near-wall velocity gradient was assessed using a linear fit to the lowest velocity measurements; subsequently, the length of a nondimensional wall unit was obtained via Eq. (1). These length scales can now be used to scale coherent structures observed in the flow; conversion of metric lengths to non-dimensional wall units will be applied in a later section of analysis.

3.2. Streak behavior

Overall, the image processing techniques resulted in a coherent framework to describe streak behavior over both the hot plate and the flame. In fact, this algorithm produced a qualitative picture of streak behavior over time at a particular streamwise location. Fig. 6 displays just one example of the streak behavior downstream of the hot plate obtained at $x = 225$ mm over a duration of 5 s. Realizing that the y-axis displays time, the resulting graph can be conceptualized as the paths streaks would take over time if viewed through a thin stationary slit. The resulting streak traces provide a beautiful and insightful description of streak behavior. In general, streaks at this location exhibit minimal lateral movement, but they

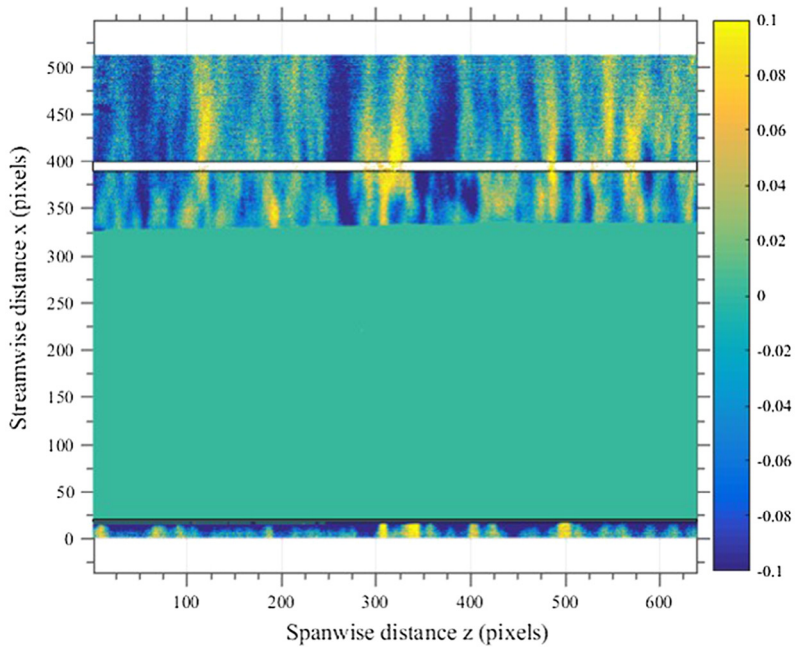

(a)

(b)

Fig. 3. (left) An example map of surface temperature fluctuations (T') generated for a test. Here, the instantaneous streak locations can be seen in yellow as positive fluctuations while troughs exist over the blue regions. All streak traces shown are found over the insulation surrounding the plate. The region over the heated plate does not display any streak traces because the temperature range of the infrared data for this example is not high enough. (right) Image of the isopropyl flame taken from the high speed overhead camera. The flow direction is from the bottom to the top of the page. The thin white box represents an example of an analysis region used at $x = 75$ mm. (For interpretation of the references to color in this figure legend, the reader is referred to the web version of this article.)

occasionally drift slightly or interact with their neighbor. This behavior contrasts with that of the flame streaks depicted in Fig. 7, which is taken at $x = 75$ mm for a period of 10 s. Here, lateral movement of the streaks is quite pronounced, and structures interact with their neighbors regularly through both merging and splitting behaviors. Most streaks also exhibit a wavy, sinuous movement, indicating that the strong buoyancy of the flame is inducing secondary flow. In fact, further downstream in the flame, streaks begin to deform into larger coherent structures possessing complex shapes. Stronger sources of buoyancy appear to significantly reduce the stability of streaks. This behavior agrees with existing mixed convection literature [22,15], which often finds that the bursting process of streaks is accelerated for a higher temperature difference.

3.3. Streak spacing

Near-wall streaks are not simply a mixed convection phenomenon; streamwise streaks are known to exist in nearly all boundary layer flows [39]. Sublayer streaks were originally discovered in turbulent flows by Kline et al. [27], but later work revealed that streaks also exist in laminar and transitional flows [40]. Near-wall streaks are a well-established phenomenon; however, they have rarely been examined in the light of mixed convection with

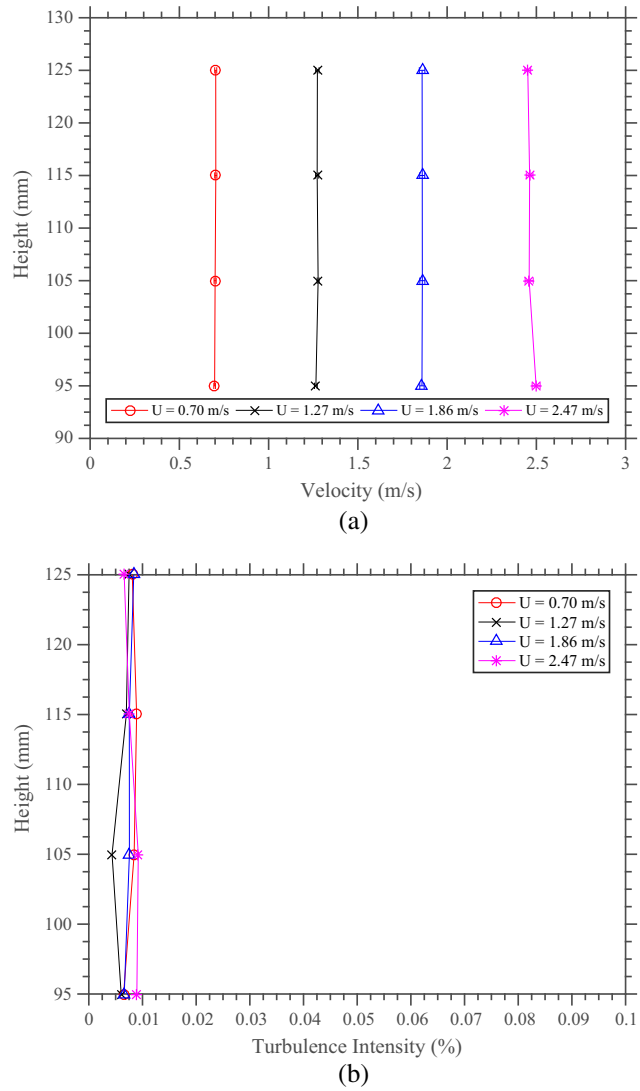

Fig. 4. (a) Plot of freestream velocity values at several heights in the center of the wind tunnel. Horizontal error bars indicate one standard deviation. (b) Plot of the turbulence intensity levels in the freestream flow at the center of the wind tunnel.

an unheated starting length or as coherent structures in combustion.

The first step in examining streak spacing involved compiling a distribution of measurements from each parameter space. In every case, the data appeared to take on a lognormal distribution. This is unsurprising, as earlier research has long suggested that streak spacing should be distributed similarly to a lognormal probability density function [28,41]. For a random variable X with μ and σ representing the mean and standard deviation of the variable's natural logarithm, the lognormal probability density function can be written as $\frac{1}{x\sigma\sqrt{2\pi}}\exp\left(-\frac{(\ln x-\mu)^2}{2\sigma^2}\right)$. A fit of this form was successfully applied to all distributions, and Fig. 8 displays several examples. Overall, the distribution can be seen to grow wider downstream, but it retains a lognormal shape.

In order to examine the adequacy of the lognormal probably density function (PDF), we compared the means and standard deviation of the experimental data to the arithmetic values associated with the lognormal fit. In Figs. 9 and 10, you can see a comparison of experimental values vs. fitted values for all tested conditions. For the majority of these statistics, all data points lie nearly adjacent to the line of unity, strongly indicating that the lognormal PDF's are adequately capturing both the centrality and variability present in derived data. In this paper, the mean has been chosen as a reported statistic; the median, which is consistently around 91% of the mean, could also have been selected and would reveal identical trends. There is some drift of the standard deviation values for downstream values of streak spacing in the flame. This occurs because the coherent structures measured in these regions are no longer truly streaklike; instead, they consist of complex shapes resulting from agglomeration of upstream streaks. This behavior can be witnessed in the image of Fig. 3.

A lognormal distribution is also commonly quantified using skewness, a measure of asymmetry about the mean, and the coefficient of variation (CV), which measures the level of dispersion. For a lognormal distribution, the skewness is equal to $(e^{\sigma^2}+2)\sqrt{e^{\sigma^2}-1}$ while the arithmetic coefficient of variation is equal to the ratio of the standard deviation to the mean, or $\sqrt{e^{\sigma^2}-1}$. No trend in these statistics was observed as the wind speed or the hot plate temperature was manipulated. However, there appears to be a positive correlation with the streamwise distance, and Figs. 11 and 12 displays a scatterplot of this relationship. Both of these values appear to increase slightly with downstream distance, indicating that there is a slightly wider dispersion of

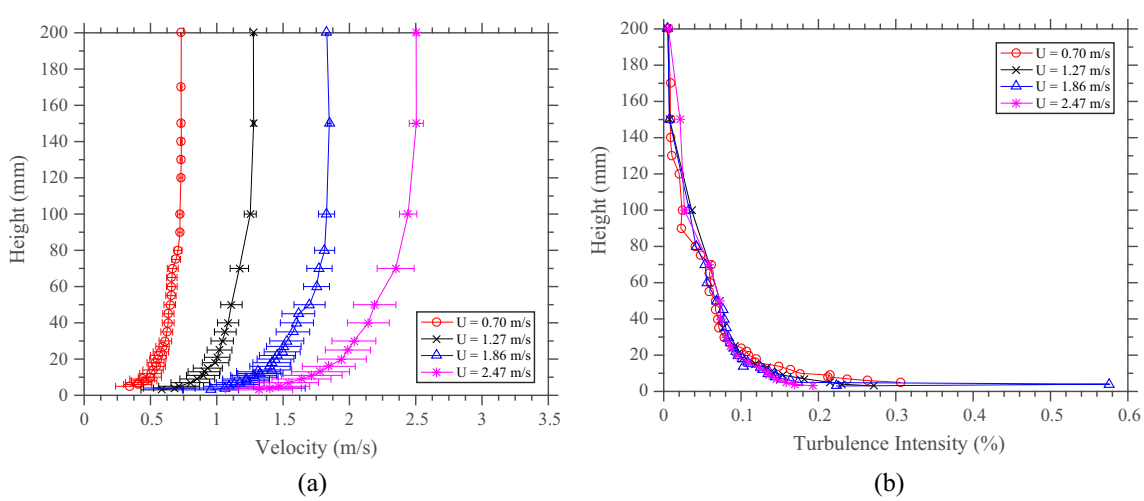

Fig. 5. (a) Height vs. velocity measured 1.5 cm upstream of the hot plate leading edge. Horizontal error bars indicate one standard deviation of the velocity data. (b) Height vs. turbulence intensities measured 1.5 cm upstream of the hot plate leading edge.

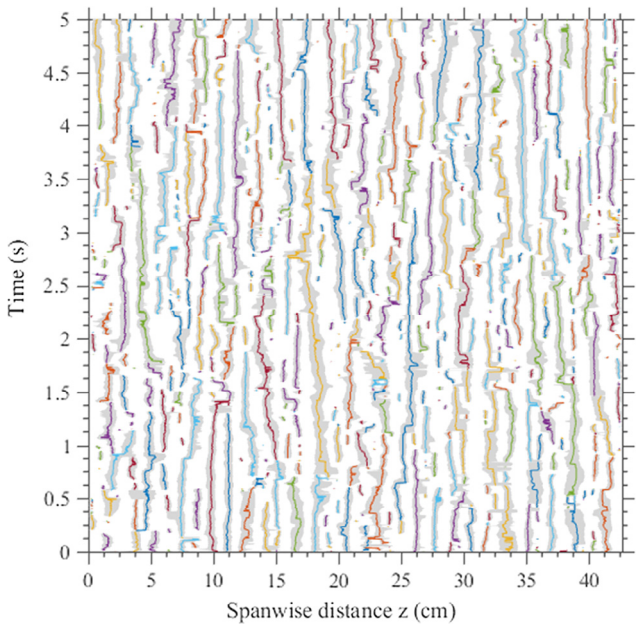

Fig. 6. Graphical illustration of streak tracking, in which the spanwise locations of streaks are plotted against time. Thin colored lines represent streak centerlines whereas light gray areas represent streak width. Data for this figure was obtained 225 mm downstream of the plate's leading edge at a wind speed of 1.27 m/s and a plate temperature of 300 °C. (For interpretation of the references to color in this figure legend, the reader is referred to the web version of this article.)

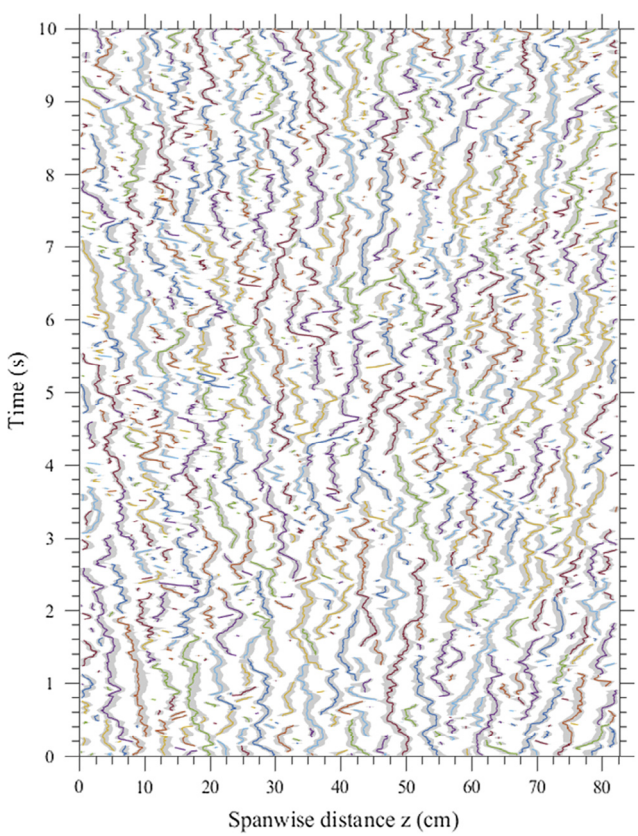

Fig. 7. Graphical illustration of streak tracking, in which the spanwise locations of streaks are plotted against time. Thin colored lines represent streak centerlines whereas light gray areas represent streak width. Data for this figure was obtained 75 mm downstream of the isopropyl flame's leading edge at a wind speed of 0.7 m/s. (For interpretation of the references to color in this figure legend, the reader is referred to the web version of this article.)

streak spacing downstream. Again, this is likely a result of the structures evolving from clear streaks to more complex structures. Several other studies [35,28,42] have also reported these statistics for distributions of near-wall streaks, but no information on the downstream trends was described.

Experimental means were extracted from all distributions, resulting in a significant amount of data for all three tested parameters: wind speed, heating, and streamwise distance. Results for the mean spacing vs. the streamwise distance (x) can be seen in Fig. 13 for all hot plate experiments and in Fig. 14 for all experiments with the isopropyl flame. In both figures, it can be seen that the streak spacing is negatively correlated to the external wind. In other words, the frequency of streaks increases with wind speed. This trend is consistently observed across the entire tested region, demonstrating that the incoming flow plays a large role in dictating the behavior of streaks.

Over the heated plate, streak spacing remains relatively constant before, above, and immediately downstream of the hot plate. However, 5 cm downstream of the hot plate ($x \approx 25$ cm) a steep rise in the spacing is observed, followed by a plateau at $x \approx 30$ cm before appearing to decrease. This behavior implies that the near-wall streaks remain relatively fixed over the heated plate, but structures appear to be growing in size downstream of the plate. This amplification is more pronounced in all cases where the hot plate temperature is higher. It is also plausible that streaks may be lifting off of the surface in this region due to the buoyant flow of the plume.

For the flame streaks, spacing is seen to increase even more remarkably as we move downstream. This is likely a consequence of the strong local source of buoyancy, which accelerates the growth of streaks. Coherent structures grow in size and regularly merge with adjacent structures downstream. This leads to a highly dynamic process, involving rapid growth and deformation of streaklike structures into more complex shapes. In fact, further downstream, it appears improper to describe the observed coherent structures as streaks.

It should be noted that the streaks observed over the hot plate, which represent near-wall structures, are not perfectly analogous to the structures in the flame, which effectively occupy a specific height in the thermal boundary layer. The flame also provides a continuous injection of heat which persists further downstream. These distinctions may serve to explain some discrepancies between results observed as we move further downstream from $x = 0$. Nevertheless, the overall behavior is quite similar, and examining both scenarios enabled quantification of effects of vastly different buoyant source strengths.

3.3.1. Initial spacing

Both inertia (wind velocity) and buoyancy (surface/flame temperature) appear to be playing a role in the streak spacing, albeit at different stages. The later growth seems to be dominated by buoyant growth, but the early stage (i.e., the initial streak spacing) appears to be tied to the inertial force. In fact, the initial spacing is likely governed by structures that already exist in the upstream boundary layer.

Fig. 15 displays a plot of this initial streak spacing vs. the Reynolds number based on L, the downstream distance from the leading edge of the apparatus to the hot plate or fuel wick. L represents the canonical length scale for flows over horizontal surfaces and is traditionally employed in similar studies because of its correlation to boundary layer growth. Clearly, a negative correlation exists between the initial streak spacing and the incoming wind speed, which is described by the Reynolds number. From another perspective, the initial streak spacing is directly related to the boundary layer height. For a higher incoming wind speed, the boundary layer height at a given streamwise location becomes shorter; con-

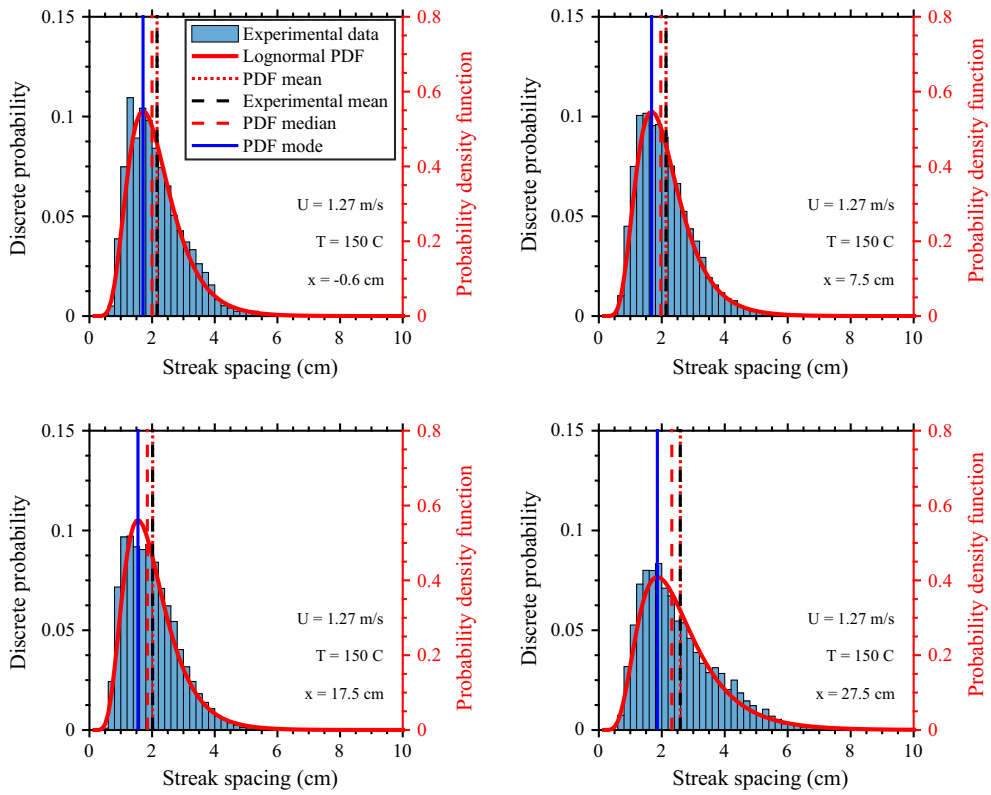

Fig. 8. Plots of experimental distributions of streak spacing along with a lognormal fit of the data. All data is taken over either the heated plate or the insulated surface where the hot plate temperature is 150 °C and the wind speed is 1.27 m/s. The indicated experimental means are derived from experimental data while other values are derived from arithmetic properties of the lognormal PDF.

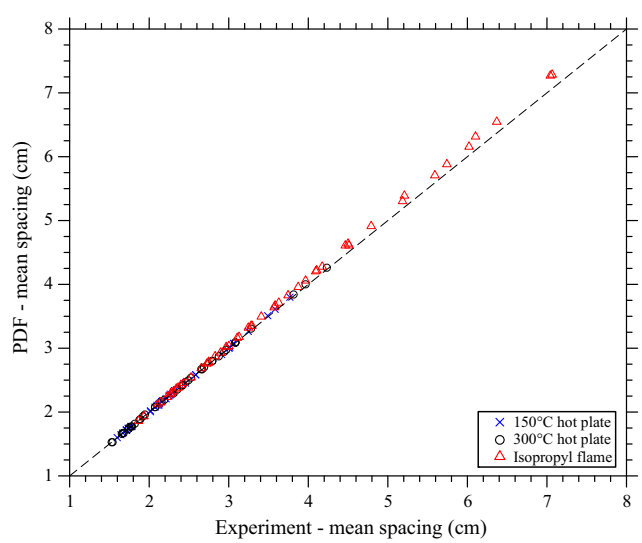

Fig. 9. Displayed here are comparisons of the mean streak spacings from the experimental data vs. the means of the fitted lognormal distribution. Data is taken from both tested hot plate temperatures as well as the isopropyl fuel wick. The dashed line indicates the line of unity.

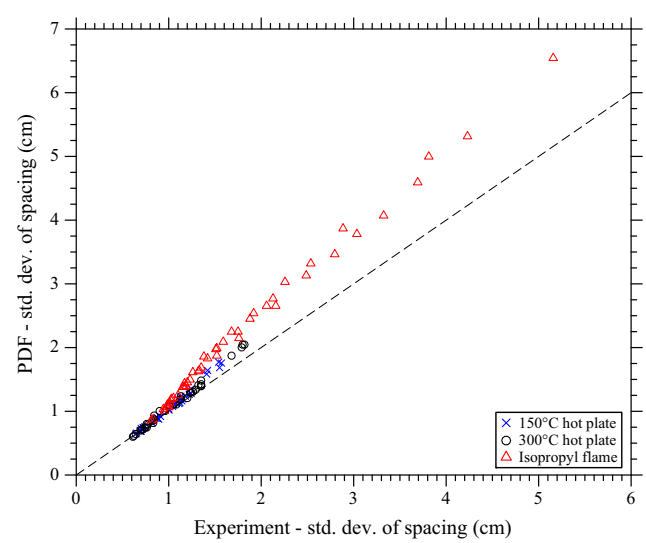

Fig. 10. This figures compares the standard deviations of spacing from the experimental data vs. those from fitted lognormal distribution. Data is taken from both tested hot plate temperatures as well as the isopropyl fuel wick. The dashed line indicates the line of unity.

sequently, the coherent structures which populate this boundary layer will also be smaller. The reported trend supports this notion, and the initial streaks appear to be preset by the incoming flow.

If the incoming boundary layer is governing the initial spacing, this length scale should agree with that expected in unheated flow. For turbulent boundary layers, near-wall streaks are typically organized into a spanwise pattern with a period of approximately 100 viscous wall units [27,43,28]. Nevertheless, there is significant variation in reported experimental values for the mean streak spacing ($\bar{\lambda}^+$), which often deviate by as much as 30 wall units from this universal value [35]. Minimal experimental data seems to exist concerning the nondimensional spacing of streaks in laminar or transitional boundary layers. However, it has been theoretically

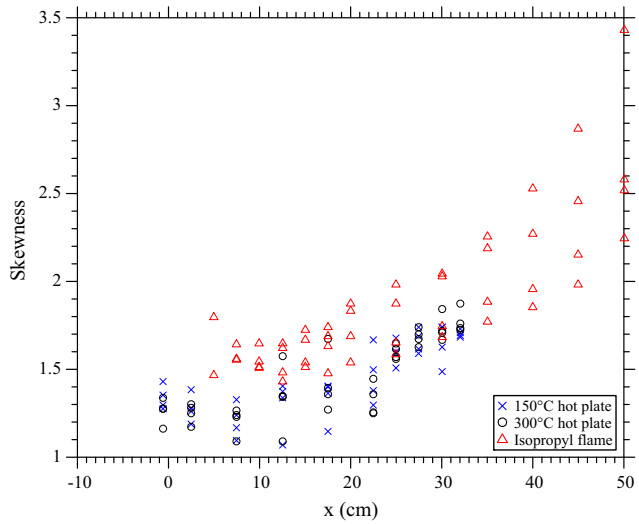

Fig. 11. Plot of the skewness vs. the streamwise distance for all tested conditions. All statistics are derived from the fitted lognormal distributions.

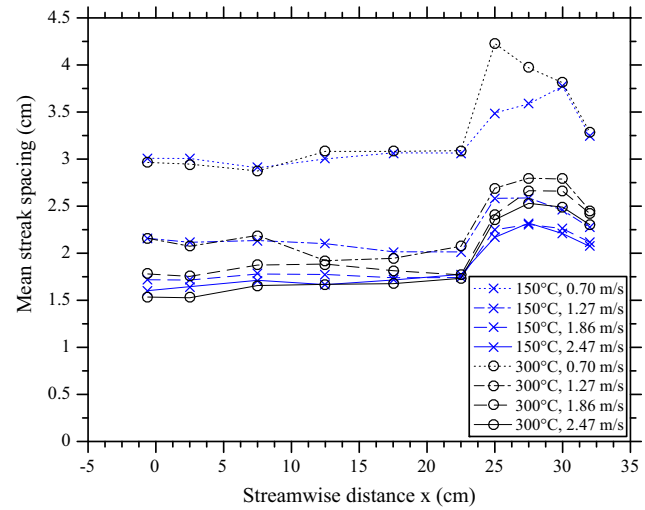

Fig. 13. Plot of the mean streak spacing vs. streamwise distance for all experimental conditions over the hot plate. The hot plate is located between $x = 0$ and 20.5 cm while the surrounding area is inert.

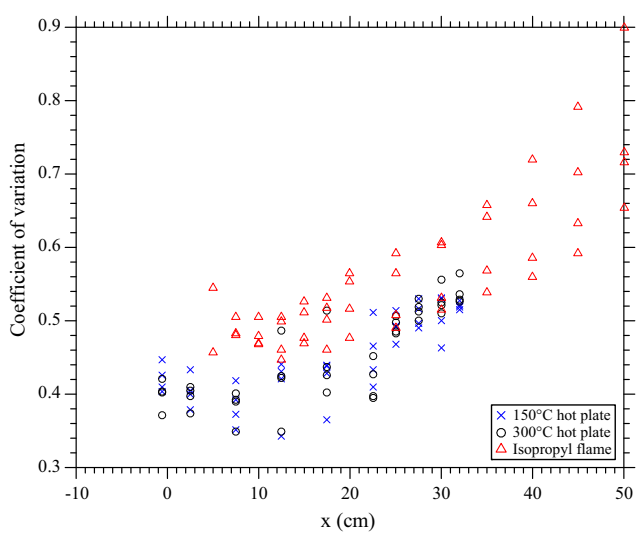

Fig. 12. Plot of the coefficient of variation vs. the streamwise distance for all tested conditions. All statistics are derived from the fitted lognormal distributions.

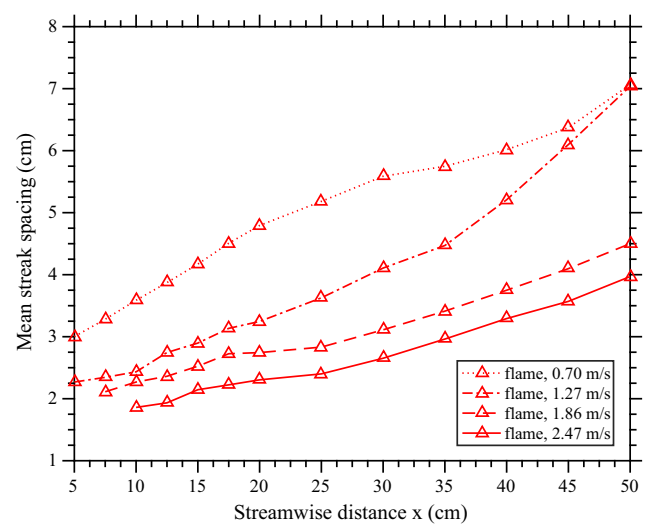

Fig. 14. Plot of the mean streak spacing vs. streamwise distance for all experimental conditions with the isopropyl fuel wick, which is located between $x = 0$ and $x = 20.5$ cm.

demonstrated that transient growth of these early coherent structures can result in the standard spacing seen in turbulent boundary layers [44]; additionally, experiments have observed quasi-linear growth of streak spacing that could hypothetically asymptote to a stable value [45]. In other words, we should not be surprised to find that the streaks in this study scale similarly to turbulent boundary layer flows. The following analysis attempts to analyze whether streak spacing here behaves similarly to those in a turbulent boundary layer, which exhibit predictable trends in non-dimensional spacing.

In order to test this hypothesis, we converted the initial streak spacing to non-dimensional wall units, and Fig. 16 displays the results of this conversion. Compared to Fig. 15, we see a remarkable collapse of the data when plotted in wall units, which are proportional to the near-wall velocity gradient. Given the immense range in the strength of the source of buoyancy, which varies from a 150 °C hot plate to an isopropyl flame, this result essentially confirms that the initial spacing is a consequence of the incoming boundary layer. The incoming coherent structures, including near-wall streaks, will be proportional to the incoming velocity boundary layer. The local buoyant force does not influence the spacing until further downstream, a finding similar to Moharerri et al. [6], who witnessed no dependence of spacing on heating in the initial stable vortex flow regime. Few studies in mixed convection have examined the effect of pre-existing disturbances which often exist upstream of the heat source, but our results indicate that they will heavily dictate the initial length scales observed.

This finding has several other important takeaways. If the spacing of structures governs the downstream development of the flame or the local heat flux to the surface, properties of the incoming boundary layer will be essential to describing these behaviors. Additionally, the universality of spacing in wall units implies that data on streak spacing can be applied to reveal properties of the incoming boundary layer. For instance, it may be possible to examine an aerial photograph of a spreading wildland fire exhibiting streaks, establish a length scale for the streak spacing, and use this data to approximate properties of the incoming boundary layer. This data could prove to be quite valuable in assessment of a wildland fire, where accurate measurements of incoming wind profiles

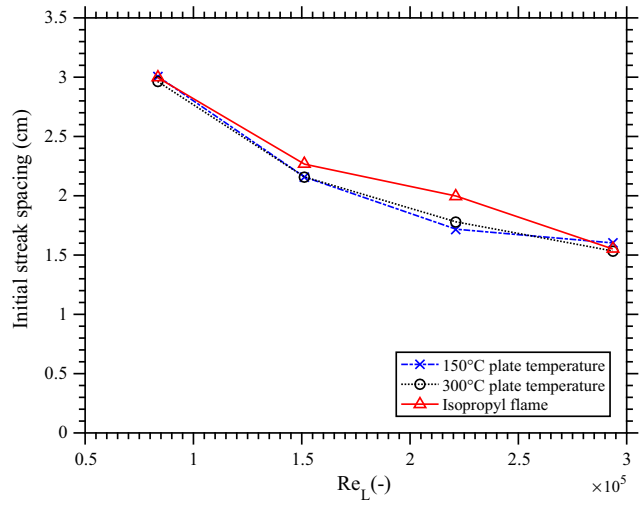

Fig. 15. A plot of the initial streak spacing vs. the Reynolds number based on L, the downstream distance from the leading edge of the apparatus to the hot plate or fuel wick.

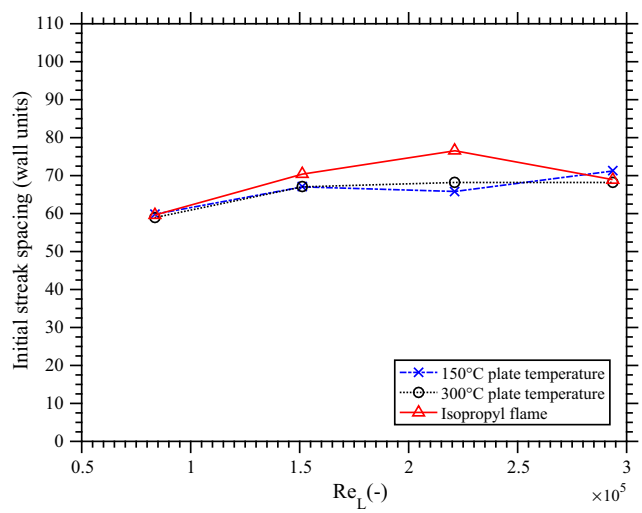

Fig. 16. A plot of the initial streak spacing in dimensionless wall units vs. the Reynolds number based on L, the downstream distance from the leading edge of the apparatus to the hot plate or fuel wick.

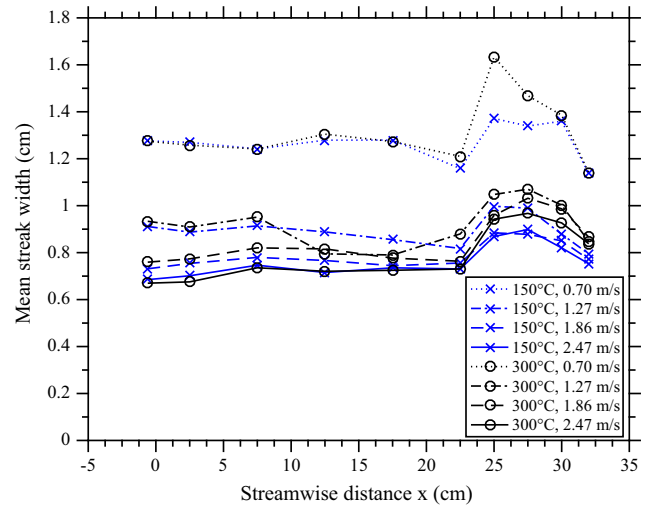

Fig. 17. A plot of the mean width of streaks vs. streamwise distance for all experimental conditions. The hot plate is located between $x = 0$ and 20.5 cm while the surrounding area is inert.

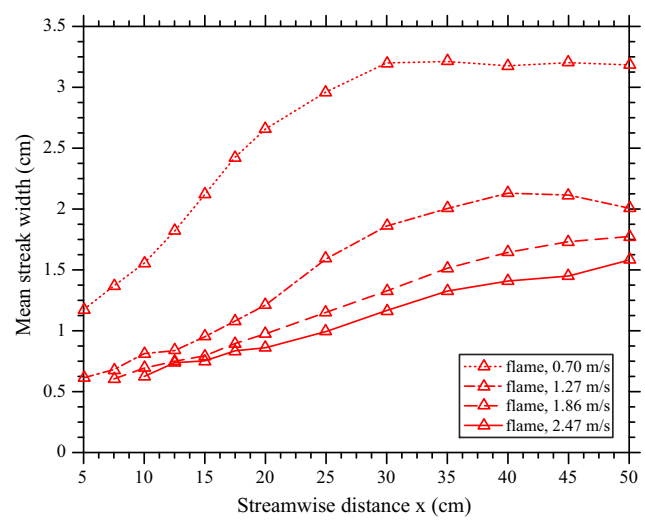

Fig. 18. A plot of the mean width of flame streaks vs. streamwise distance for all wind speeds. The isopropyl fuel wick is located between $x = 0$ and $x = 20.5$ cm.

or even instantaneous wind data are often unattainable. If nothing else, the presence of streaks may indicate that a boundary layer is governing the incoming flow and will modify the behavior of the flame.

3.4. Streak width

In addition to the spacing between streaks, the width of streaks was also tabulated. This was done for the entire parameter space, and all distributions of width were seen to follow a lognormal trend, similar to the spacing. Additionally, the trends for width remained identical to the streaks when the mean values were plotted vs. the streamwise distance in Figs. 17 and 18. The widths identified by the detection algorithm consistently occupy about 40–50% of the spacing, which is similar to results from the edge detection method of Zachsenhouse et al. [35].

The width of streaks is negatively correlated to the wind speed and is seen to increase downstream; both of these trends were observed for the spacing as well. However, there appears to be an asymptote reached for the width of streaks in the flame at a certain downstream distance. This can be observed around 30 cm for a wind speed of 0.70 m/s and around 40 cm for a wind speed of 1.27 m/s. Similar behavior was observed by Zuercher et al. [22], who observed that, after initial quasi-exponential growth, the vortex size became saturated. The asymptotic behavior of the flame streak width could be due to the fact that downstream measurements are taken towards the outer extents of a flame, where most of the flammable gases have already reacted. Alternatively, it is possible that there are limitations on the width of these coherent structures which will restrict growth despite a constant increase in spacing between these structures. This behavior is likely related to the peak and trough structure of a flame, which has been shown to be correlated to the flame length [23]. It appears that there is a settling of length scale which is based on the time for growth of structures. This time scale is positively correlated to the flame length, which enables growth, and negatively correlated to the wind speed, which determines the time structures inhabit the flaming region. A time scale based on the flame length (or burning depth) and the wind speed may be related to the largest observed length scale

of coherent structures; further research would help to show how this phenomena modifies the heat transfer to the surface at the furthest extents of a flame. It should be noted that for a semi-infinite hot plate or flame there will be no dominant length scale; growth and mixing will occur indefinitely. The behavior seen here is likely only reproducible when the heated source, such as a hot plate or a flame, is finite in length.

3.5. Streak interaction

The detection algorithm was able to track instances where streaks and other coherent structures would deform or interact with adjacent structures. Splitting instances, where a larger structure would divide into two smaller structures, and merging instances, where two smaller structures would combine to form a larger structure, were tabulated for all conditions in the isopropyl flame. Results are displayed in Figs. 19 and 20. Further downstream, the number of instances of splitting and merging both increase dramatically, indicating that the flow is becoming more chaotic and adjacent structures are more heavily influenced by their neighbors. Furthermore, the ratio of merging to splitting increases downstream, indicating that streaks have a higher propensity to combine and form larger length scales downstream. This agrees with the increase in length scales previously reported.

4. Conclusion

This study examined the behavior of mixed convection streaks appearing in boundary layer flows with an unheated starting length. The behavior of coherent structures in this configuration, which is commonly observed in real flows, was probed by manipulating the incoming wind speed or the local buoyant source, which was provided by either a hot plate or a diffusion flame. An algorithm for tracking and quantifying streak behavior was developed and successfully employed to determine important trends.

The onset of the streaks was confirmed to be controlled by the coherent structures populating the incoming boundary layer. This initial length scale was entirely independent of the strength of the buoyant source, whether it was supplied by a 150 °C hot plate or an isopropyl flame. The streak spacing was normalized in wall units, indicating that the near-wall velocity gradient is strongly correlated to the observed structures. This indicates that the initial spacing in the presence of an unheated starting length can be understood via theory for unheated flows. Properties of the incoming boundary layer or knowledge of potential upstream disturbances will be essential to describing initial behavior. Observations of initial streak spacing can also be used to estimate properties of the incoming flow, particularly in situations such as wildfires, where flow properties are difficult to attain.

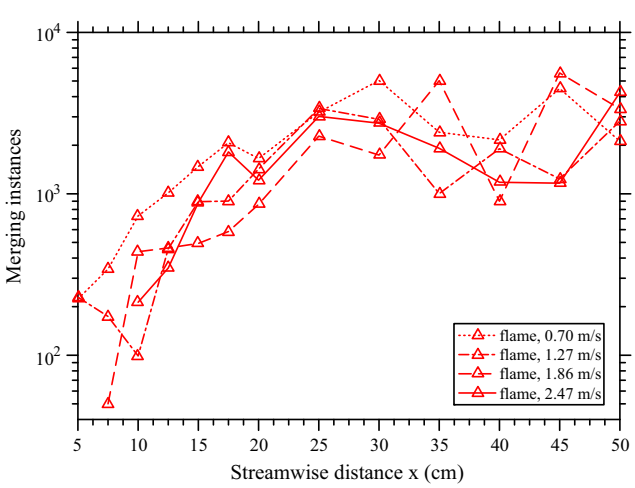

Fig. 19. A semilogarithmic plot of the instances of streak merging observed in a 5 s period. The isopropyl fuel wick is located between $x = 0$ and $x = 20.5$ cm.

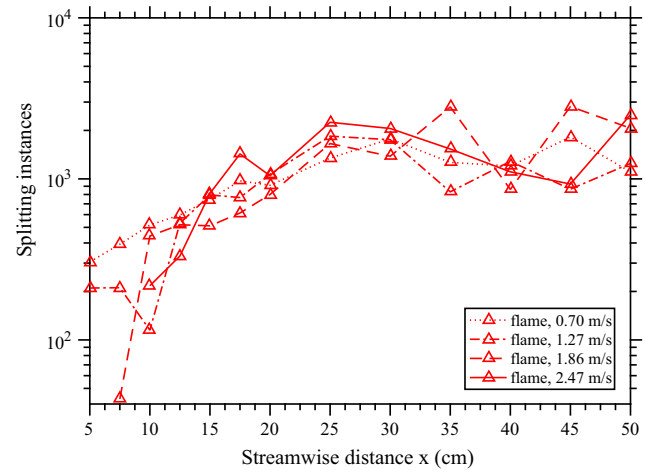

Fig. 20. A semilogarithmic plot of the instances of streak splitting observed in a 5 s period. The isopropyl fuel wick is located between $x = 0$ and $x = 20.5$ cm.

After the initial onset, buoyancy begins to play a dominant role in the streak behavior. Both the spacing and the width grow downstream due to buoyant amplification of these instabilities. Knowledge of the rate and duration of buoyant growth can be used to describe the amplification of structures. In particular, the width of flame streaks appears to saturate after a certain time due to the time scales associated with buoyant growth over a finite distance. The rate of growth is likely a function of the density difference between the cold flow and the heated flow, indicating that theory for buoyant instability growth (i.e., Rayleigh-Taylor scaling) is applicable. Previous research by the author [21] has indicated that the quadratic growth of Rayleigh-Taylor instabilities is a plausible avenue of scaling the downstream growth.

Finally, the downstream development of the streaks indicates transition from a stable flow with three dimensional longitudinal disturbances to a highly chaotic turbulent flow possessing complex coherent structures. The initial flow in the near-wall region is governed by the streaks observed in mixed convection, but amplification and destabilization of these structures enables transition to turbulent flow. Because the length of heating is finite, the mean length scales appear to saturate, meaning that resolving heat and mass transfer in this region may require knowledge of these scales. In summary, the downstream evolution of coherent structures in heated boundary layer flow appears to be governed primarily by the initial disturbances and the length and time scales associated with buoyant growth. This has significant implications for applications involving mixed convection with an unheated starting length, particularly in scenarios such as wildland fires where surface heat transfer and plume length scales are important. CFD simulations of similar boundary layer phenomena should consider whether the associated structures and the upstream disturbances are accurately resolved. Future research is needed to validate other regimes of behavior; in particular, it would be useful to further examine the role upstream disturbances play in more fully-developed turbulent boundary layer and on atmospheric scales. Several of the configurations depicted in Fig. 1 represent instances where this question would be relevant, and further tests could examine these regimes. Knowledge of the incoming velocity field and the near-wall structures will remain essential to understanding the evolution of these

structures. Analogous behavior likely remains restricted to boundary layer phenomena; regardless, this exploratory research project has certainly challenged the two-dimensional formulation typically used to describe mixed convection. It is our hope that this project provides a strong framework for future investigations.

Conflicts of interest

None declared.

Acknowledgments

The authors would like to acknowledge financial support for this work from the USDA Forest Service Missoula Fire Sciences Laboratory through the National Fire Decision Support Center under collaborative agreement 13-CS-11221637-124 and from the National Science Foundation under award CBET 1554026. The authors would like to sincerely thank the support we received from the technicians and researchers at the Missoula Fire Sciences Laboratory, including Torben Grumstrup, Josh, Randy, John, Andrew, and Cyle. Finally, significant insights were provided by our colleagues Dr. Arnaud Trouvé and Salman Verma, who contributed incredibly constructive comments during our discussions.

Appendix A. Detection algorithms

In infrared images taken from hot plate tests, streaks that form over the hot plate and the surrounding inert material (which has been warmed by conduction) create alternating regions of heating and cooling over the surface that can be visualized through post-processing. This phenomenon is a consequence of the counter-rotating streamwise vortices, where downwash regions of vortex pairs pulls cooler air from the ambient flow downward toward the heated surface. This fluid then cools the surface, creating a local region of decreased temperature. Consequently, an alternating pattern of heating and cooling on the surface that can be detected from infrared images. In this experiment, streak spacing is on the order of one centimeter, so significant spatial resolution is necessary in order to resolve this phenomenon. We found that a resolution of 640 × 512 pixels covering a region roughly 42 cm × 35 cm accurately resolved the streak spacings. Additionally, the streaks are seen to rapidly meander across the surface, which means that the sampling frequency of the associated infrared camera must be high enough to capture the instantaneous streak traces instead of washing out this motion. A frame rate of 280 Hz proved more than adequate for this purpose. Finally, the infrared camera must be sensitive enough to detect the magnitudes of these minute temperature changes.

Images from 5 s of video were used to determine a time-averaged image, which revealed a mean temperature map of the surface. Next, the temperature fluctuation, or T', was calculated for each frame and each pixel via the equation $T'|_{t=t_1} = \frac{T(t_1)}{\overline{T}}$, where $T'|_{t=t_1}$ is T' at a single time $t_1, T(t_1)$ is the instantaneous temperature, and $\overline{T}$ is the mean temperature over the sampling period. The sensitivity of the mean surface temperature ($\overline{T}$) to the averaging period was determined to be adequate.

A MATLAB program would then scan through each frame subsequently. A map of T' for one frame would be generated for the user to enable confirmation that the program was analyzing the correct region and at a position where streak traces could be seen (see Fig. 3). Because the IR camera can only operate in a single temperature range at one time, temperature measurements over the hot plate at 150 °C and 300 °C were captured via temperature filters of 80–200 °C and 150–350 °C, respectively. Temperature measurements made over the surrounding insulated region at 150 and 300 °C were possible with temperature filters of 35–150 and 80–200 °C, respectively. Conversions from lengths in pixels to lengths in cm was made possible by measuring the depth of the hot plate in the derived images, and a conversion factor of 15.0 pixels/cm proved adequate. Since the camera angle was not modified between tests, the leading edge of the hot plate was consistently located approximately 19 pixels from the bottom edge of the image, meaning that this location could be normalized as $x = 0$ cm. All other streamwise distances were then normalized using this reference point and the conversion factor. The user was instructed to input a specific streamwise location (in cm) to analyze, and this method enabled determination of the appropriate row of pixels to examine. Once this row was determined, a relevant region of the data above and below was selected in order to smooth out inconsistencies. The selection region was always 11 pixels (0.73 cm) in depth (i.e., 5 pixels (0.33 cm) above and 5 pixels below the user-indicated region).

Once the selection region was confirmed, a single spanwise temperature profile for T' was established by averaging the raw T' data in the streamwise direction. In other words, if the selection region was 640 pixels in width and 11 pixels in depth, all T' data would be averaged over the depth, resulting in an array with 640 data points for each frame. Next, the MATLAB program would run through all frames in order to identify streaks in each T' profile. Significant work went into fine-tuning this analysis so that it could be consistently applied to all data regardless of profile characteristics. The T' profile was first smoothed, with a smoothing span of 5 pixels (approximately 0.33 cm). MATLAB's pre-existing command *findpeaks*, was then used to detect local maxima, but inputs had to be specified in order to reliably detect peaks. Specifying a minimum peak prominence, as determined by MATLAB's algorithm, proved to be most reliable because it eliminated peaks that were small while retaining peaks that were indicative of streaks. It should be noted that the determination of prominence by MATLAB differs from the determination of streak amplitude, which is defined later. The minimum prominence height was determined by looking at the T' profile, pulling out the standard deviation, and specifying the minimum prominence as 50% of the standard deviation. In this way, the minimum height was established as being proportional to the fluctuations observed in the signal, and it seemed to be fairly robust as it could be seen to reliably detect most streaks and eliminate most noise. For each test, the user would be presented with results from 5 separate images to confirm that the detection algorithm was working as intended.

In addition to identifying the location of the streaks for each image, it was also desirable to look at streak width, streak amplitude, and streak spacing. The streak spacing was simply determined by tabulating the distance between peaks of adjacent streaks. The streak amplitude was determined by the following method: minimum values in the T' signal between the analyzed streak and its adjacent neighbors to the left and right would be indexed; from here, the amplitude was evaluated to be the difference between the T' value at the streak (necessarily a peak in the data) and the larger of the left or right minimum values. The streak width would then be determined by the following method: the raw T' value between the larger of the left or right minimums and the peak value would be assessed and termed the *midval*; next, the algorithm would move left from the peak value at the streak to find where the signal was less than or equal to the midval - this would be the left extent of the streak; the algorithm would repeat this process to the right to identify the right extent of the streak; the width was then selected as the distance between the left and right extents. It should be noted that widths and amplitudes are determined separate from MATLAB's *findpeaks* command.

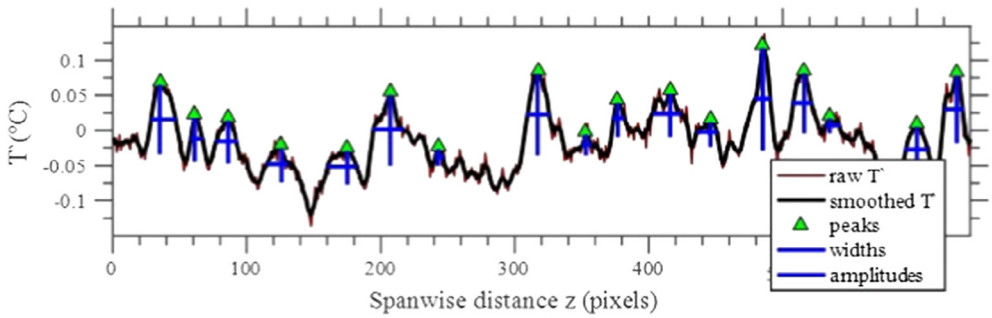

Fig. 21. Example of the streak detection algorithm with displayed results for one image. Here, the raw T' profile is shown as a thin red line while the smoothed profile is shown as the thicker black line. This image also shows derived streak locations or peaks (green triangles), streak widths (horizontal blue lines), and streak amplitudes (vertical blue lines). (For interpretation of the references to color in this figure legend, the reader is referred to the web version of this article.)

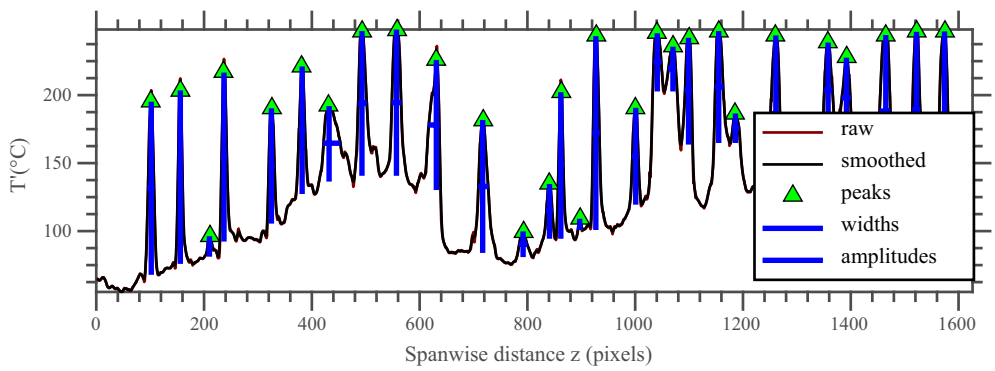

Fig. 22. Example of the streak detection algorithm with displayed results for one image. Here, the raw luminosity profile is shown as a thin red line while the smoothed profile is shown as the thicker black line. This image also shows derived streak locations or peaks (green triangles), streak widths (horizontal blue lines), and streak amplitudes (vertical blue lines). (For interpretation of the references to color in this figure legend, the reader is referred to the web version of this article.)

Fig. 21 shows the final results of this process for an example frame, where the streak locations, widths, and amplitudes are overlaid on top of the T' profile. It can be seen that there are a couple smaller fluctuations in the data that could be accepted as streaks if the sensitivity of the algorithm was increased. However, examination of Fig. 21 clearly indicates that the detection algorithm is working at an adequate level, especially given that it can be consistently applied for all input conditions, including plate temperature, wind speed, and streamwise location. When averaged over 1400 images a consistent distribution of data was derived.

In order to track the movement of streaks, it would be intuitive to posit that, between two consecutive frames, the most likely candidate as a match for a streak in the first frame is the one that is spatially nearest in the second frame. This intuition was applied to the compiled data, enabling assessment of the lateral movement of streaks was assessed. A lateral velocity for the streak was then calculated as the distance traveled by the streak divided by the time between frames. The maximum distance a streak could be observed to obtain a match was established as 85% of the mean streak width, and this dynamic criterion proved repeatable over the parameter space. When two streaks from a previous frame both matched with a streak from the future frame, the closer streak was matched. This scenario, in which streaks would appear to combine forming an inverse 'V' shape, constitutes a streak merging event, and the location and time of this event were recorded. In addition, if one streak from a previous frame obtained two possible matches in the next frame which were not closer to any other pre-existing streaks, a splitting event would occur. This behavior, which was also recorded, is visualized as a 'V' shape in the streak traces. Finally, the birth and deaths of streaks was also tabulated. When a streak obtained no matches in the subsequent frame or if its only matches were closer to other pre-existing streaks, the lifetime of the streak would be terminated. Additionally, when a streak appeared in a subsequent frame that had no proper matches from the previous frame, it was determined to be a new streak. By assessing this birthing and dying process, it was possible to attach lifetimes to streaks.

The infrared images taken over the hot plate were slightly obscured due to the background electrical noise of the alternating current providing power. This noise, visualized in a Fast Fourier Transform (FFT), which displays a signal in the frequency domain, produced active bands at approximately 30 and 60 Hz. Consequently, bandpass filtering was employed for data taken from the heated region ($x = 0$–20.5 cm). The filter was designed as a band-stop infinite impluse response (IIR filter) directed towards the relevant frequencies (approximately 30 and 60 Hz). Derived data from this region is less accurate than that of the inert regions, and filtering the signal resulted in artificially reduced streak amplitudes. For this reason, discussion or tabulation of final results occasionally excludes data over the hot plate.

For experiments on the isopropyl fuel wick, detecting streaks consists simply in identifying the luminous regions of the flame. In other words, the detection method applied to the hot plate is directly applicable if the spanwise T' profile is replaced with a spanwise profile of luminous intensity. Fig. 22 displays a plot of this detection algorithm used over the intensity profile taken from a high-speed video. The peak-finding algorithm works exactly the same with a couple of small tweaks to the input parameters: the number of pixels/cm was equal to 19.67; the duration of the analysis was 10 s (1363 frames); the streamwise depth of the analysis region was 7 pixels; the percentage of the standard deviation used

as a minimum for peak prominence was 15%; the maximum movement of a continuous streak between frames was 85% of its width. Finally, a small portion on the left and right sides of the images were ignored in the analysis because the flame was only intermittently present in these areas. Even greater detail on the streak detection algorithms is presented in the author's thesis [46].

Appendix B. Supplementary material

Supplementary data associated with this article can be found, in the online version, at https://doi.org/10.1016/j.ijheatmasstransfer.2017.11.040.

References

[1] E. Pohlhausen, Der wärmeaustausch zwischen festen körpern und flüssigkeiten mit kleiner reibung und kleiner wärmeleitung, ZAMM-J. Appl. Math. Mech./Zeitschrift für Angewandte Mathematik und Mechanik 1 (2) (1921) 115–121.
[2] R. Gilpin, H. Imura, K. Cheng, Experiments on the onset of longitudinal vortices in horizontal blasius flow heated from below, J. Heat Transfer 100 (1) (1978) 71–77.
[3] Y. Mori, Buoyancy effects in forced laminar convection flow over a horizontal flat plate, J. Heat Transfer 83 (4) (1961) 479–482.
[4] E. Sparrow, W.J. Minkowycz, Buoyancy effects on horizontal boundary-layer flow and heat transfer, Int. J. Heat Mass Transfer 5 (6) (1962) 505–511.
[5] T. Chen, E. Sparrow, A. Mucoglu, Mixed convection in boundary layer flow on a horizontal plate, J. Heat Transfer 99 (1) (1977) 66–71.
[6] S.S. Moharreri, B.F. Armaly, T. Chen, Measurements in the transition vortex flow regime of mixed convection above a horizontal heated plate, J. Heat Transfer 110 (2) (1988) 358–365.
[7] X. Wang, An experimental study of mixed, forced, and free convection heat transfer from a horizontal flat plate to air, J. Heat Transfer 104 (1) (1982) 139–144.
[8] Y. Hayashi, A. Takimoto, K. Hori, Heat transfer in laminar, mixed convection flow over a horizontal flat plate, in: Proceedings of the 14th Japan Heat Transfer Symposium, 1977, pp. 4–6.
[9] J. Yoo, P. Park, C. Choi, S. Ro, An analysis on the thermal instability of forced convection flow over isothermal horizontal flat plate, Int. J. Heat Mass Transfer 30 (5) (1987) 927–935.
[10] T. Sengupta, S. Unnikrishnan, S. Bhaumik, P. Singh, S. Usman, Linear spatial stability analysis of mixed convection boundary layer over a heated plate, Prog. Appl. Math. 1 (1) (2011) 71–89.
[11] R.-S. Wu, K. Cheng, Thermal instability of blasius flow along horizontal plates, Int. J. Heat Mass Transfer 19 (8) (1976) 907–913.
[12] A. Moutsoglou, T. Chen, K. Cheng, Vortex instability of mixed convection flow over a horizontal flat plate, ASME, Trans., J. Heat Transfer 103 (1981) 257–261.
[13] K. Chen, M. Chen, Thermal instability of forced convection boundary layers, ASME J. Heat Transfer 106 (1984) 284–289.
[14] H. Imura, R. Gilpin, K. Cheng, An experimental investigation of heat transfer and buoyancy induced transition from laminar forced convection to turbulent free convection over a horizontal isothermally heated plate, J. Heat Transfer 100 (3) (1978) 429–434.
[15] K. Cheng, T. Obata, R. Gilpin, Buoyancy effects on forced convection heat transfer in the transition regime of a horizontal boundary layer heated from below, J. Heat Transfer 110 (3) (1988) 596–603.
[16] M.-H. Lin, Numerical study of formation of longitudinal vortices in natural convection flow over horizontal and inclined surfaces, Int. J. Heat Mass Transfer 44 (9) (2001) 1759–1766.
[17] H. Shaukatullah, B. Gebhart, An experimental investigation of natural convection flow on an inclined surface, Int. J. Heat Mass Transfer 21 (12) (1978) 1481–1490.
[18] K. Kitamura, F. Kimura, Heat transfer and fluid flow of natural convection adjacent to upward-facing horizontal plates, Int. J. Heat Mass Transfer 38 (17) (1995) 3149–3159.
[19] H. Görtler, Über eine analogie zwischen den instabilitäten laminarer grenzschichtströmungen an konkaven wänden und an erwärmten wänden, Arch. Appl. Mech. 28 (1) (1959) 71–78.
[20] R. Biertümpfel, H. Beer, Natural convection heat transfer increase at the laminar-turbulent transition in the presence of instationary longitudinal vortices, Int. J. Heat Mass Transfer 46 (16) (2003) 3109–3117.
[21] C.H. Miller, W. Tang, M.A. Finney, S.S. McAllister, J.M. Forthofer, M.J. Gollner, An investigation of coherent structures in laminar boundary layer flames, Combust. Flame 181 (2017) 123–135.
[22] E. Zuercher, J. Jacobs, C. Chen, Experimental study of the stability of boundary-layer flow along a heated, inclined plate, J. Fluid Mech. 367 (1998) 1–25.
[23] M.A. Finney, J.D. Cohen, J.M. Forthofer, S.S. McAllister, M.J. Gollner, D.J. Gorham, K. Saito, N.K. Akafuah, B.A. Adam, J.D. English, Role of buoyant flame dynamics in wildfire spread, Proc. Nat. Acad. Sci. 112 (32) (2015) 9833–9838.
[24] E. Weckman, A. Strong, Experimental investigation of the turbulence structure of medium-scale methanol pool fires, Combust. Flame 105 (3) (1996) 245–266.
[25] P. DesJardin, T. Smith, C. Roy, Numerical simulations of a methanol pool fire, in: 39th Aerospace Sciences Meeting and Exhibit, 2001, p. 636.
[26] D. Gorham, R. Hakes, A. Singh, J. Forthofer, J. Cohen, S. McAllister, M. Finney, M. Gollner, Studying wildland fire spread using stationary fires, in: D.X. Viegas (Ed.), VII International Conference on Forest Fire Research, 2014.
[27] S. Kline, W. Reynolds, F. Schraub, P. Runstadler, The structure of turbulent boundary layers, J. Fluid Mech. 30 (4) (1967) 741–773.
[28] C. Smith, S. Metzler, The characteristics of low-speed streaks in the near-wall region of a turbulent boundary layer, J. Fluid Mech. 129 (1983) 27–54.
[29] Q.X. Lian, A visual study of the coherent structure of the turbulent boundary layer in flow with adverse pressure gradient, J. Fluid Mech. 215 (1990) 101–124.
[30] M. Rashidi, S. Banerjee, Streak characteristics and behavior near wall and interface in open channel flows, J. Fluids Eng. 112 (2) (1990) 164–170.
[31] G. Hetsroni, R. Rozenblit, Heat transfer to a liquidsolid mixture in a flume, Int. J. Multiphase Flow 20 (4) (1994) 671–689.
[32] D. Kaftori, G. Hetsroni, S. Banerjee, Funnel-shaped vortical structures in wall turbulence, Phys. Fluids 6 (9) (1994) 3035–3050.
[33] B. Achia, D. Thompson, Structure of the turbulent boundary in drag-reducing pipe flow, J. Fluid Mech. 81 (03) (1977) 439–464.
[34] D. Sabatino, Instantaneous Properties of a Turbulent Spot in a Heated Boundary Layer.
[35] M. Zacksenhouse, G. Abramovich, G. Hetsroni, Automatic spatial characterization of low-speed streaks from thermal images, Experim. Fluids 31 (2) (2001) 229–239.
[36] G. Fortuna, T.J. Hanratty, The influence of drag-reducing polymers on turbulence in the viscous sublayer, J. Fluid Mech. 53 (03) (1972) 575–586.
[37] A. Gupta, J. Laufer, R. Kaplan, Spatial structure in the viscous sublayer, J. Fluid Mech. 50 (03) (1971) 493–512.
[38] D. Spalding, A single formula for the law of the wall, J. Appl. Mech. 28 (3) (1961) 455–458.
[39] R.L. Panton, Overview of the self-sustaining mechanisms of wall turbulence, Prog. Aerosp. Sci. 37 (4) (2001) 341–383.
[40] K. PS, Effect of free-stream turbulence on a laminar boundary layer, in: Bulletin of the American Physical Society, vol. 16, 1971, p. 1323.
[41] H. Nakagawa, I. Nezu, Structure of space-time correlations of bursting phenomena in an open-channel flow, J. Fluid Mech. 104 (1981) 1–43.
[42] K.A. Flack, Near-wall structure of three-dimensional turbulent boundary layers, Experim. Fluids 23 (4) (1997) 335–340.
[43] J. Klewicki, M.M. Metzger, E. Kelner, E. Thurlow, Viscous sublayer flow visualizations at r_θ = 1,500,000, Phys. Fluids (1994–present) 7 (4) (1995) 857–863.
[44] B.F. Farrell, P.J. Ioannou, Dynamics of streamwise rolls and streaks in turbulent wall-bounded shear flow, J. Fluid Mech. 708 (2012) 149.
[45] S.-C. Deng, C. Pan, J.-J. Wang, Dynamics of low-speed streak evolution and interaction in laminar boundary layer, Acta Mech. Sin. 30 (5) (2014) 636–645.
[46] C.H. Miller, Fluid Dynamics of Boundary Layer Combustion, Ph.D. thesis, University of Maryland, 2017.